RSC Advances

PAPER

View Article Online
View Journal | View Issue

Cite this: *RSC Adv.*, 2022, **12**, 9051

Bimetal phosphide as high efficiency and stable bifunctional electrocatalysts for hydrogen and oxygen evolution reaction in alkaline solution†

Yutong Liu,‡[a] Meng Ding, ‡*[a] Xiaolong Deng,[b] Yafang Zhang[a] and Gang Zhao [a]

The development of low-cost, high-efficiency, and stable bifunctional electrocatalysts for large-scale water electrolysis is very important for the sustainable development of energy. In this paper, the nickel cobalt phosphide (CoNiP) microstructure was prepared by the *"in situ* growth-ion exchange-phosphating" method. Due to the flake structure and the synergistic effect of the bimetal, the synthesized CoNiP microstructure exhibited high electrocatalytic activity and stability for hydrogen and oxygen evolution in alkaline electrolyte. The optimized CoNiP showed low overpotential of 116 mV at 10 mA cm^{-2} for hydrogen evolution reaction and 400 mV at 50 mA cm^{-2} for oxygen evolution reaction in KOH solution. In addition, it exhibited long-term stability at a high constant current density of 100 mA cm^{-2} for 48 hours at room temperature and for 65 hours at 80 °C without significant degradation. Theoretical results showed that the introduction of Co and P atoms could reduce the reaction barrier and improve the electron transfer ability. This work provides a simple and economical way for the synthesis of electrocatalytic bimetal phosphide catalysts.

Received 7th January 2022
Accepted 14th March 2022

DOI: 10.1039/d2ra00099g

rsc.li/rsc-advances

1. Introduction

With the development of global industrialization, energy becomes an indispensable resource in human life. As traditional energy is greatly consumed, which mainly comes from non-renewable resources, human beings are already facing the problem of energy depletion.[1] Hydrogen has the apparent advantages of being a clean, broad resource, having high energy density, and being sustainable,[2] and also it is an ideal energy carrier. The production of hydrogen as an important research direction of hydrogen energy application has been widely investigated by researchers all over the world. Electrochemical decomposition of water is considered as one of the cleanest ways to produce hydrogen.[3] It is an important research topic in the field of decomposing water to produce hydrogen and oxygen with low electric energy by creating a highly efficient electrocatalyst. Overall, water decomposition is divided into anodic oxygen evolution reaction and cathodic hydrogen evolution reaction.[4] At present, Ir/Ru and Pt are considered to be much better catalysts for the OER and HER.[5,6] However, the scarcity and high cost of noble metals limit their practical application as efficient electrocatalysts. In order to overcome these problems, non-precious metal electrocatalysts with excellent electrocatalytic performance and low cost are chosen to replace these precious metal catalysts. The bifunctional catalysts are active for both hydrogen evolution reaction (HER) and oxygen evolution reaction (OER) reactions, which are more conducive to practical application.[7] Therefore, it is of great practical significance to develop economical, efficient and bifunctional electrocatalysts.

Transition metals and their oxide, sulfide,[8] selenide,[9] phosphide,[10] nitride[11] are considered as promising bifunctional electrocatalytic materials because of their abundant reserves and low cost. Especially, transition metal phosphides have been extensively studied due to their high catalytic activity and electrical conductivity.[12–16] For example, Yang *et al.* synthesized nanosheet self-assembled NiCoP microflowers as efficient bifunctional catalysts in alkaline medium.[17] Yin *et al.* prepared NiCoP on nickel foam with intertwined and porous columnar morphology, which showed superior HER and OER performance.[18] Zeng *et al.* fabricated 3D flower-like clusters of CoNiP nanofoils grown on randomly-dispersed rGO-nanosheets with superior electrocatalysis for hydrogen evolution reactions.[19] Furthermore, some research groups have studied the electrocatalytic activity of compounds based on CoNiP. Shao *et al.* synthesized CoNiP@layered double hydroxides core–shell nanosheets arrays as bifunctional electrocatalyst.[20] Although some achievements have been achieved with nanostructured metallic phosphides, their electrocatalytic activity can be improved by adjusting geometric structures.[21] Additionally,

[a]School of Physics and Technology, University of Jinan, 336 Nanxinzhuang West Road, Jinan, 250022, People's Republic of China. E-mail: sps_dingm@ujn.edu.cn
[b]School of Mathematics and Physics, Anhui University of Technology, Ma'anshan 243032, Anhui, People's Republic of China

† Electronic supplementary information (ESI) available. See DOI: 10.1039/d2ra00099g

‡ These authors contributed equally to this work.

researchers prefer to prepare self-supporting electrodes for direct application in water electrolysis cells, which can simplify the equipment of water electrolysis and potentially reduce the cost.[22,23]

In this paper, the self-supporting bimetal phosphide CoNiP catalyst is prepared through three steps (etching, ion exchange and phosphating) on foamed nickel. The layered structure of the microstructure affords abundant active sites and provides enough space for the diffusion of the electrolyte to accelerate the release of bubbles. In addition, CoNiP shows much better electrocatalytic performance after ion exchange in cobalt nitrate solution. Furthermore, the CoNiP catalyst shows superior durability with little change after constant current measurement for 48 hours at room temperature and 65 hours at 80 °C.

2. Results and discussion

The CoNiP/NF electrocatalyst is synthesized by three steps of "*in situ* growth-ion exchange-phosphating", as shown in Fig. 1a. The SEM images of $Ni(OH)_2$, $Ni_xCo_{1-x}OH$, Ni_2P and CoNiP are displayed in Fig. 1b–e. It can be seen that $Ni(OH)_2$ with strip structure is formed after etching by hydrochloric acid and immersing in deionized water. Note that after ion exchange, the morphology of product changes to spike-like structure. Finally, a lamellar layered structure appears after phosphating, and the thickness of CoNiP nanosheets is about 21 nm, which is displayed in Fig. S1.† The TEM images of CoNiP with high magnification in Fig. 1f–h display the fringe spacings of 0.22 nm and 0.202 nm, corresponding well to the (111) and (201) crystal plane of CoNiP,[24,25] which further confirms successful synthesis of CoNiP. The EDS element mapping images (Fig. 1i–l) verify the existent of Ni, Co, and P elements, and distributed uniformly in the lamellar layered structure.

The X-ray diffraction (XRD) is used to study the crystal structure of as-synthesized samples. As shown in Fig. S2,† the diffraction peaks of CoNiP/NF-0.15 M centered at 40.99°, 44.90° and 47.58° can be assigned to the (111), (201) and (210) plane of hexagonal CoNiP (marked with triangle, PDF: 71-2336). The result is consistent with the TEM image in Fig. 1h, which could further confirm the existence of CoNiP. For comparison, the crystalline Ni_2P sample is prepared. The diffraction peak of Ni_2P (Fig. 2b) located at 40.71°, 44.61° and 54.20° could be well

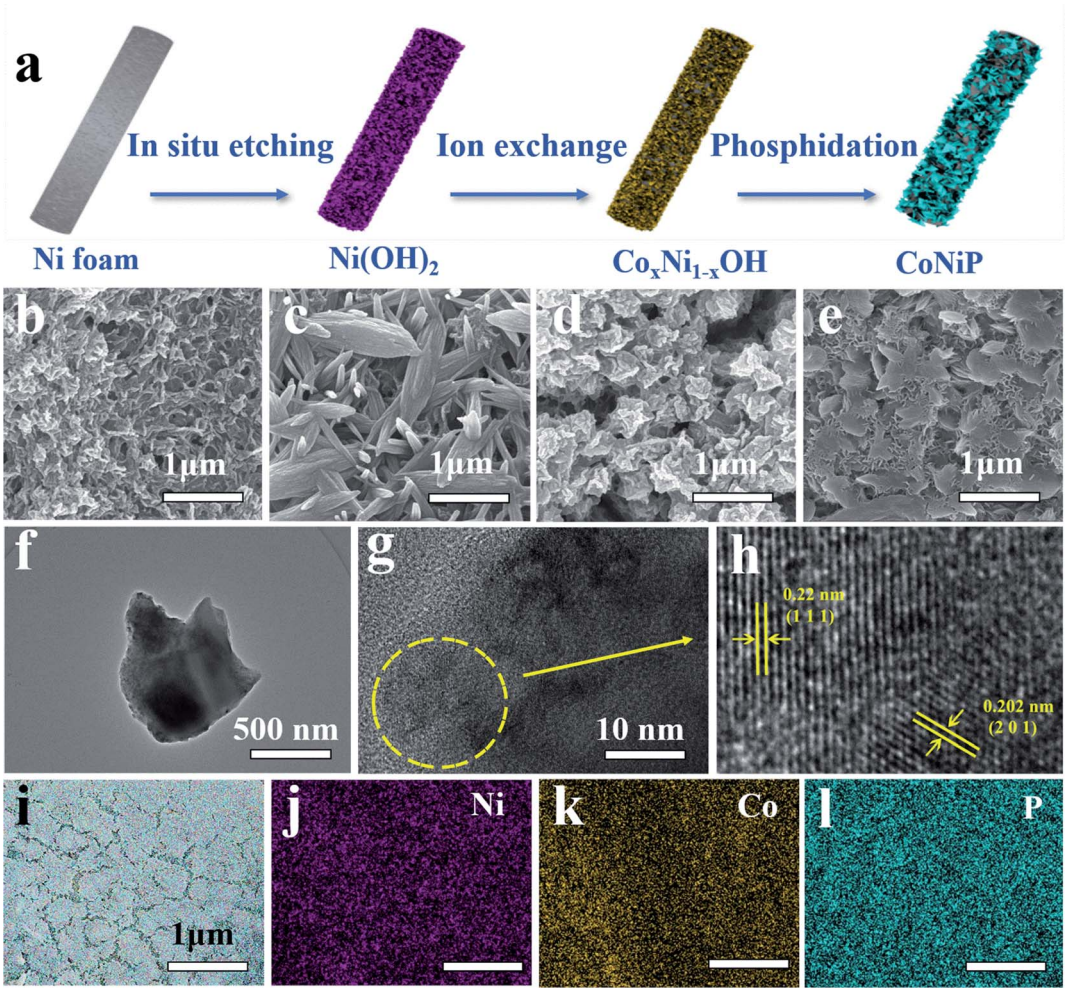

Fig. 1 (a) Schematic diagram of CoNiP/NF formation process. SEM images of (b) $Ni(OH)_2$/NF, (c) $Co_xNi_{1-x}OH$/NF, (d) Ni_2P/NF and (e) CoNiP-0.15 M/NF. (f) TEM, (g) and (h) HRTEM images. (i) SEM image of CoNiP and the corresponding EDX element mapping images of (j) Ni, (k) Co, and (l) P.

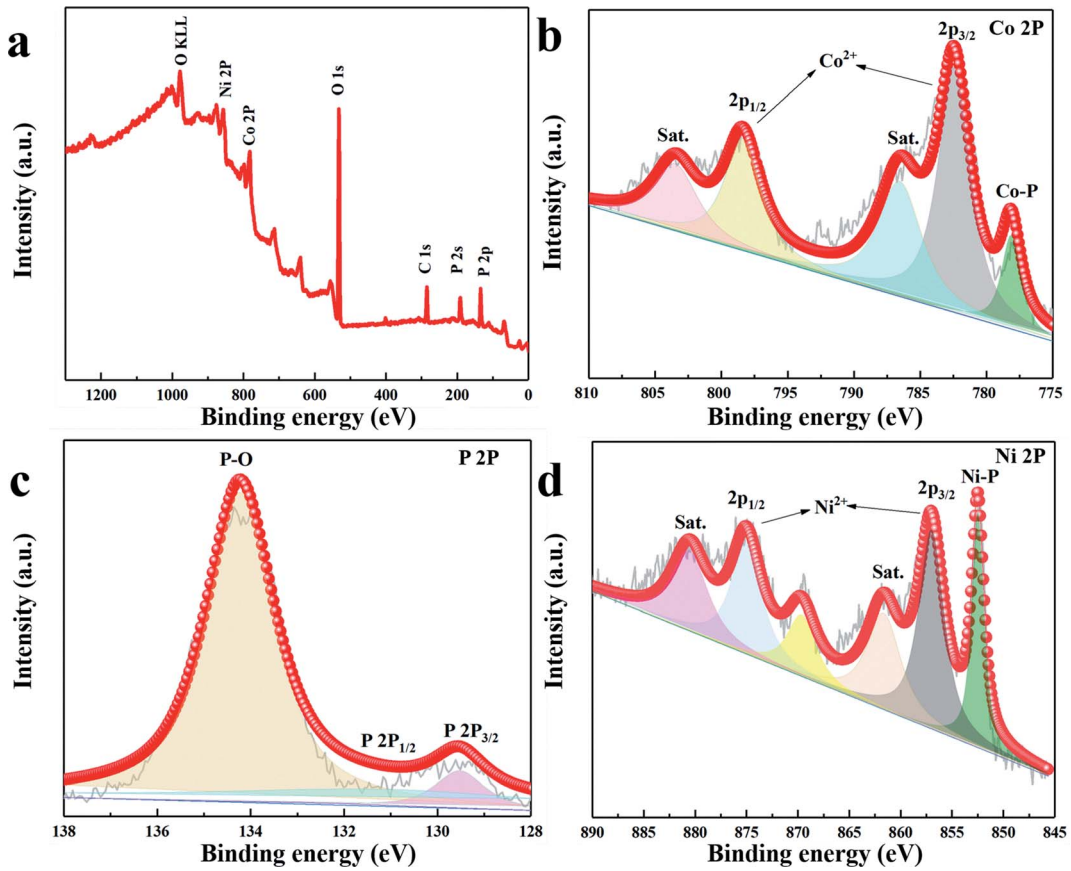

Fig. 2 (a) XPS survey spectrum of CoNiP-0.15 M. High-resolution (b–d) XPS spectra of the Co 2p, P 2p and Ni 2p for the CoNiP-0.15 M microstructure.

indexed to (111), (201), (002) crystal planes of hexagonal Ni_2P (marked with asterisk, PDF: 03-0953).

In order to study the surface chemical composition of CoNiP microstructure, X-ray photoelectron spectroscopy depth profile analysis was carried out. As shown in Fig. 2a, the characteristic peaks of nickel, cobalt and phosphorus elements clearly appear in the XPS survey spectrum of CoNiP. The high-resolution XPS spectrum of Co element is depicted in Fig. 2b, and two obvious peaks located at 782.5 eV and 798.5 eV in the Co 2p spectrum can be assigned to Co $2p_{2/3}$ and Co $2p_{1/2}$, which are accompanied by two satellite peaks at 786.7 eV and 803.5 eV. Moreover, the peak located at 778.2 eV can be attributed to the Co–P bond.[26] As presented in Fig. 2c, the binding energy of about 130.1 and 129.4 eV can be ascribed to P–Ni or P–Co bond in P $2p_{1/2}$ and P $2p_{3/2}$, respectively. In addition, the strong oxidation peak located at 134.2 eV is assigned to the P–O bond because of the air exposure.[24,26] In Fig. 2d, the two obvious peaks at 857.1 eV and 875.1 eV are attributed to Ni $2p_{2/3}$ and Ni $2p_{1/2}$, meanwhile, the satellite peaks of Ni $2p_{2/3}$ and Ni $2p_{1/2}$ at 861.7 eV and 880.6 eV are observed. Furthermore, the peak with binding energy at about 853.7 eV is ascribed to the Ni–P bond.[26,27] The XPS result corresponds well to the XRD of the sample, which further illustrates the successful synthesis of CoNiP.

The HER and OER electrocatalytic activity of all samples are evaluated in 3.0 M KOH at room temperature. For HER electrocatalytic activity, as shown in Fig. 3a, the LSV curves exhibit that the CoNiP/NF-0.15 M electrocatalyst possesses excellent catalytic activity compared with other samples. As Fig. 3b shown, the overpotential of the prepared CoNiP/NF-0.15 M is 116 mV at 10 mA cm^{-2}, which is lower than that of Ni_2P (149.5 mV), $Co_xNi_{1-x}(OH)$ (174.5 mV), $Ni(OH)_2$ (178.5 mV), indicating that the introduction of Co ions and P ions has significantly improved catalytic performance of samples.[28,29] For bimetal phosphide, the content of metal ions has influence on the performance of electrocatalyst. Therefore, in order to investigate the effect of Co amount on the HER performance, the LSV curves of CoNiP with three different concentrations of cobalt nitrate solution are studied (shown in Fig. 3c). Among these catalysts, the CoNiP-0.15 catalyst exhibits the best HER activity, and the overpotential is 61 and 24 mV lower than that of CoNiP-0.1 M, CoNiP-0.2 M, respectively. In order to further evaluate catalytic activity of as-fabricated samples, the catalytic kinetics are analysed using the corresponding Tafel plots computed from LSV data in Fig. 3a. The Tafel slope is fitted by the following Tafel equation:

$$\eta = b \log|j| + a$$

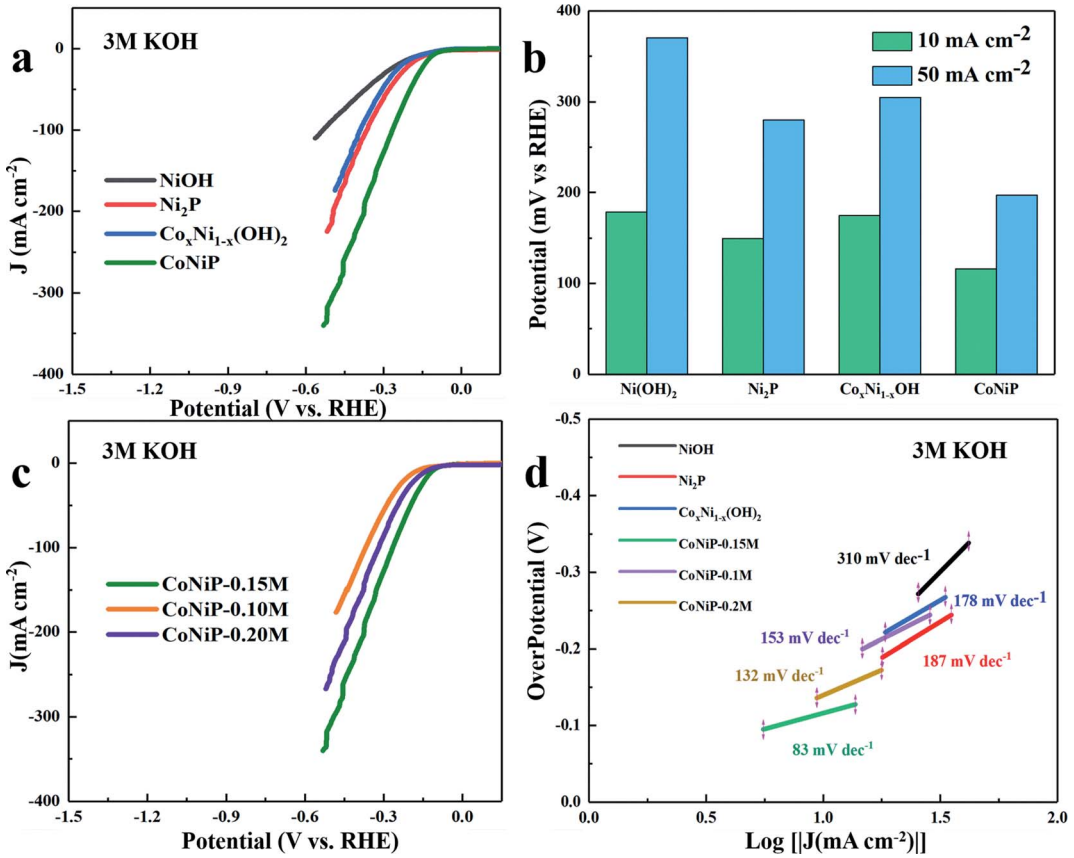

Fig. 3 (a) HER LSV curves of as-fabricated samples. (b) The summarized overpotential at 10 mA cm^{-2} and 50 mA cm^{-2}. (c) HER LSV curves of CoNiP/NF samples with three different concentrations of cobalt nitrate solution (0.15 M, 0.1 M, 0.2 M). (d) Tafel plots. All the measurements are performed in 3 M KOH electrolyte at room temperature.

where j represents the current density and b is the Tafel slope. As shown in Fig. 3d, it can be clearly seen that CoNiP/NF-0.15 M exhibits the smallest Tafel slope of 83 mV dec^{-1}, which is much lower than Ni_2P (187 mV dec^{-1}), $Co_xNi_{1-x}(OH)$ (178 mV dec^{-1}) and $Ni(OH)_2$ (310 mV dec^{-1}). It implies that the heterometallic site CoNiP obviously improves the catalytic activity of Ni_2P.[30]

The OER catalytic activity of CoNiP is also investigated in alkaline solution (3 M KOH), and the LSV curve is compared with Ni_2P, $Co_xNi_{1-x}(OH)$, $Ni(OH)_2$. As shown in Fig. 4a, an obvious oxidation peak at about 1.4 V in the LSV curves of CoNiP/NF-0.15 M, Ni_2P/NF, $Co_xNi_{1-x}OH$/NF and $Ni(OH)_2$/NF samples can be observed, which is attributed to the oxidation–reduction reaction of Co^{2+}/Co^{3+} or Ni^{2+}/Ni^{3+} in these catalysts.[26,27,31] Similarly, CoNiP/NF-0.15 M electrocatalyst possesses superior catalytic activity for OER. Furthermore, the CoNiP/NF-0.15 M requires overpotential of about 400 mV to achieve the current density of 50 mA cm^{-2}, which is smaller than 474 mV of Ni_2P and 426 mV of $Co_xNi_{1-x}OH$, indicating that CoNiP/NF-0.15 M has relatively excellent OER catalytic activity (Fig. 4b). The LSV curves of CoNiP synthesized with different concentrations of cobalt nitrate are observed in Fig. 4c. Obviously, the synthesized CoNiP-0.15 M has a lower overpotential at the same current density, which is 57 and 20 mV lower than that of CoNiP-0.1 M, CoNiP-0.2 M, implying that it possesses much better OER performance. As shown in Fig. 4d, the Tafel slopes of CoNiP/NF-0.15 M, Ni_2P/NF, $Co_xNi_{1-x}(OH)$/NF and $Ni(OH)_2$/NF are 122, 164, 133 mV dec^{-1}, respectively. The improved electrocatalytic activity of CoNiP is probably due to the synergistic effects between Ni and Co, which can strengthen the polarization of Ni and Co electrons and make them easier to adsorb OH^- ions, and then accelerate reaction kinetics that is in favour of OER performance.[32]

The electrochemical impedance spectroscopy analyses of as-grown samples are shown in Fig. 5a, the CoNiP/NF-0.15 M exhibits smaller Nyquist semicircle diameter compared with other electrocatalysts, indicating much smaller charge transfer resistance and faster electron transport rate. In order to evaluate the durability of the CoNiP/NF-0.15 M electrocatalyst in 3 M KOH, sequential chronopotentiometric measurement at 100 mA cm^{-2} is performed at room temperature (as shown in Fig. 5b), and there is only negligible voltage changes after the 48 hour continuous test. Especially, the durability of the CoNiP/NF-0.15 M at 80 °C is evaluated, and the overpotential increases by about 18 mV after 65 hours of continuous testing, which indicates that the material has excellent stability.

Density functional theory calculations are carried out to investigate the mechanism of enhanced HER performance of CoNiP. Fig. 6a and b shows the side and top view of the

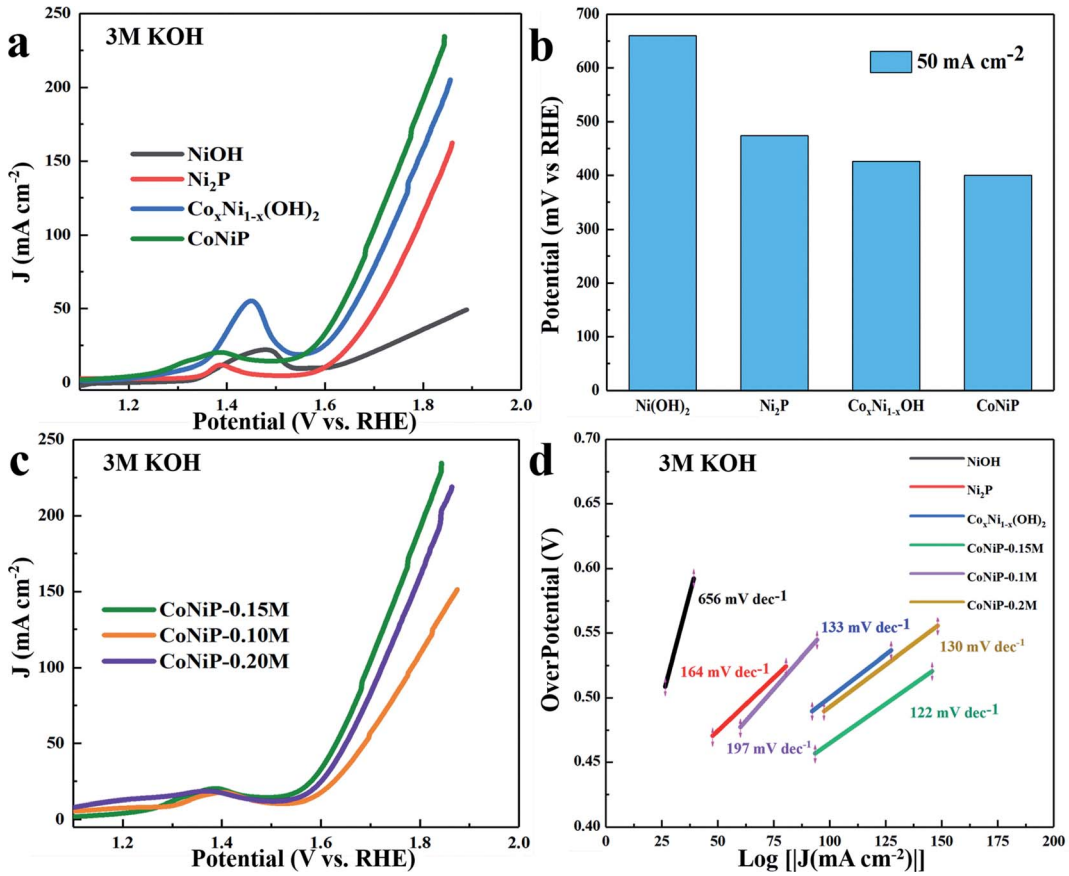

Fig. 4 (a) OER LSV curves of as-fabricated s samples. (b) The summarized overpotential under current density of 50 mA cm^{-2}. (c) OER LSV curves of CoNiP samples with three different concentrations of cobalt nitrate solution (0.15 M, 0.1 M, 0.2 M). (d) Tafel plots. All the measurements are performed in 3 M KOH electrolyte at room temperature.

geometric structure of CoNiP, respectively. In our calculation, the optimization of structure shows that the best adsorption position of hydrogen atom in CoNiP is the top site of cobalt atom. We calculate the density of states (DOS) of the non-adsorbed surface to analyze their electronic structures. Compared with Ni_2P, CoNiP shows significant increase in DOS at Fermi level (Fig. 6d), inferring that the introduction of Co element can improve the ability of electric conduction of the material. Moreover, we perform Bader's charge population analysis on both CoNiP and Ni_2P. As shown in Fig. 6e, The adsorption site of Co (CoNiP) loses more electrons than that of Ni (Ni_2P), and the *H on CoNiP gains more electrons than that

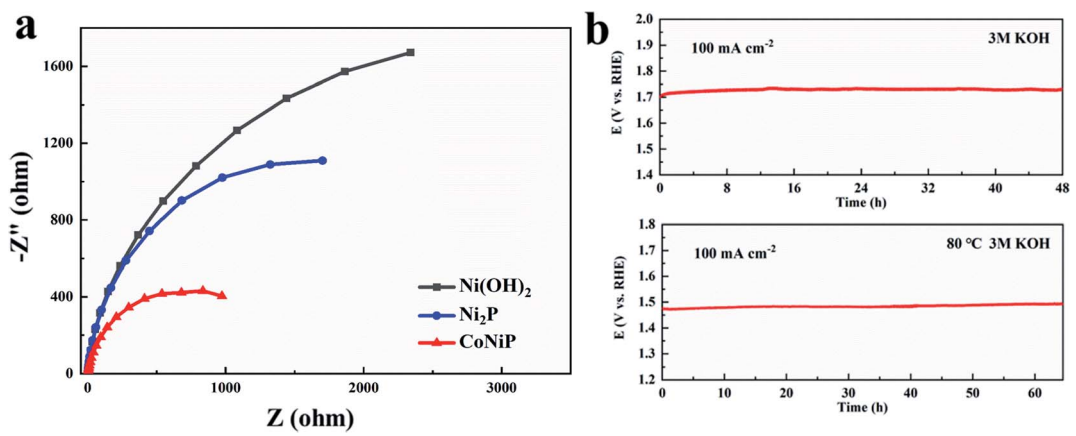

Fig. 5 (a) Nyquist plots of $Ni(OH)_2$/NF, Ni_2P/NF, and CoNiP/NF samples. (b) Chronopotentiometric curve of CoNiP/NF at 100 mA cm^{-2} in 3 M KOH electrolyte at room temperature and 80 °C, respectively.

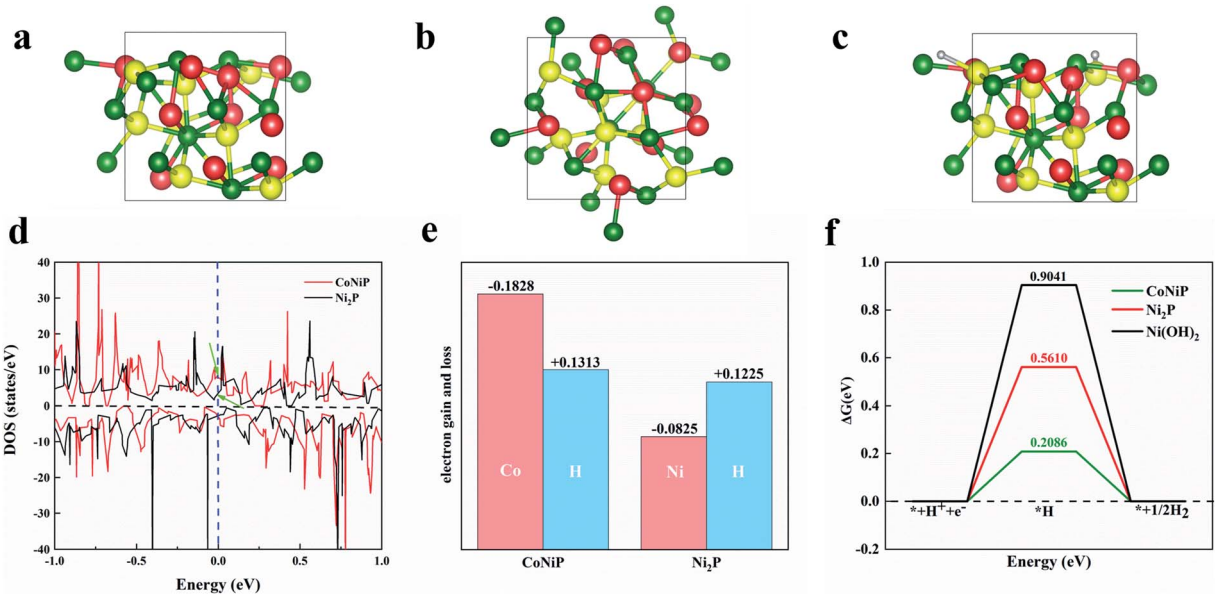

Fig. 6 Structure model of CoNiP (a) side view and (b) top view. (c) Optimized HER *H adsorbed on CoNiP. Note that the color of gray, yellow, red and green stand for H, Co, Ni and P atoms, respectively. (d) The total DOS of CoNiP and Ni_2P. (e) Electron gain and loss of adsorption site and H atom in CoNiP and Ni_2P. (f) Overpotential for CoNiP, Ni_2P and $Ni(OH)_2$.

on Ni_2P, which indicates that CoNiP has stronger electron transfer ability than Ni_2P, and enhances the bonding between the adsorption site and *H. The Gibbs free energy is also calculated and plotted in Fig. 6f. It can be seen that Ni_2P has a higher (positive) Gibbs free energy (ΔG = 0.5610 eV) for adsorption of H, while CoNiP has a relatively lower potential barrier (ΔG = 0.2086 eV), which indicates that the bonding between Ni_2P and *H is too weak for the HER, and the introduction of Co atom could enhance the bonding and therefore reduce the overpotential of HER. According to the analysis above, it is the improvement of electric conduction and enhancement of charge transfer, both of which are due to the doping of Co atoms, that promote the formation of *H on CoNiP surface.

3. Conclusion

A facile strategy to prepare CoNiP microstructure by the three-step method of "*in situ* growth-ion exchange-phosphating" was proposed. In the catalytic process, CoNiP-0.15 M showed the best catalytic performance. The overpotential of HER at 10 mA cm^{-2} is 116 mV, and that of OER at 50 mA cm^{-2} is 400 mV. In addition, it can be electrolyzed at a constant high current density of 100 mA cm^{-2} for 48 hours at room temperature and for 65 hours for 80 °C without significant degradation, showing that it has excellent stability. Theoretical results show that the introduction of Co and P atoms can obviously reduce the reaction barrier and improve the electron transfer ability.

Conflicts of interest

There are no conflicts to declare.

Acknowledgements

Y. T. Liu and M. Ding contributed equally to this work. The authors thanks eceshi (www.eceshi.com) for the SEM, XRD, XPS, TEM experiments.

References

1 G. T. Xiang, Y. Meng, G. M. Qu, J. M. Yin, B. Teng, Q. Wei and X. J. Xu, *Sci. Bull.*, 2020, **65**, 443–451.
2 J. A. Turner, *Science*, 2004, **305**, 972–974.
3 Y. Liang, Y. Li, H. Wang and H. Dai, *J. Am. Chem. Soc.*, 2013, **135**, 2013–2036.
4 L. A. Stern, L. Feng, F. Song and X. Hu, *Energy Environ. Sci*, 2015, **8**, 2347–2351.
5 G. Chen, T. Wang, J. Zhang, P. Liu, H. Sun, X. Zhuang, M. Chen and X. Feng, *Adv. Mater.*, 2018, **30**, 1706279.
6 Y. Wei, X. Zhang, Z. Wang, J. Yin, J. Huang, G. Zhao and X. Xu, *Chinese Chem. Lett.*, 2021, **32**, 119–124.
7 X. Chia and M. Pumera, *Nat. Catal.*, 2018, **1**, 909–921.
8 D. Kong, J. J. Cha, H. Wang, H. R. Lee and Y. Cui, *Energy Environ. Sci*, 2013, **6**, 3553–3558.
9 K. Li, J. Zhang, R. Wu, Y. Yu and B. Zhang, *Adv. Sci.*, 2016, **3**, 1500426.
10 Q. Liu, J. Tian, W. Cui, P. Jiang, N. Cheng, A. M. Asiri and X. Sun, *Angew. Chem., Int. Ed.*, 2014, **53**, 6710–6714.
11 X. Jia, Y. Zhao, G. Chen, L. Shang, R. Shi, X. Kang, G. I. Waterhouse, L. Z. Wu, C. H. Tung and T. Zhang, *Adv. Energy Mater.*, 2016, **6**, 1502585.
12 Y. Li, Z. Dong and L. Jiao, *Adv. Energy Mater.*, 2020, **10**, 1902104.
13 J. Tian, Q. Liu, A. M. Asiri and X. Sun, *J. Am. Chem. Soc.*, 2014, **136**, 7587–7590.

14 L. Gan, M. Heggen, R. O'Malley, B. Theobald and P. Strasser, *Nano Lett.*, 2013, **13**, 1131–1138.
15 F. Yu, H. Zhou, Y. Huang, J. Sun, F. Qin, J. Bao, W. A. Goddard, S. Chen and Z. Ren, *Nat. Commun.*, 2018, **9**, 1–9.
16 Y. Xin, X. Kan, L. Y. Gan and Z. Zhang, *ACS Nano*, 2017, **11**, 10303–10312.
17 T. Chen, M. Qian, X. Tong, W. Liao, Y. Fu, H. Dai and Q. Yang, *Int. J. Hydrogen Energy*, 2021, **46**, 29889–29895.
18 J. Guo, Z. Zhan, T. Lei and P. Yin, *Int. J. Hydrogen Energy*, 2022, **47**, 5974–5989.
19 M. Huang, K. Ge, G. Dong, Z. Zhou and Y. Zeng, *Int. J. Hydrogen Energy*, 2019, **44**, 13195–13204.
20 L. Zhou, S. Jiang, Y. Liu, M. Shao, M. Wei and X. Duan, *ACS Appl. Energy Mater.*, 2018, **1**, 623–631.
21 G. Li, X. Zhang, H. Zhang, C. Liao and G. Jiang, *Appl. Catal. B Environ.*, 2019, **249**, 147–154.
22 X. Zhang, W. Gu and E. Wang, *Nano Res.*, 2017, **10**, 1001–1009.
23 Y. P. Zhu, Y. P. Liu, T. Z. Ren and Z. Y. Yuan, *Adv. Funct. Mater.*, 2015, **25**, 7337–7347.
24 R. Zhang, X. Wang, S. Yu, T. Wen, X. Zhu, F. Yang, X. Sun, X. Wang and W. Hu, *Adv. Mater.*, 2017, **29**, 1605502.
25 W. Li, D. Xiong, X. Gao, W. G. Song, F. Xia and L. Liu, *Catal. Today*, 2017, **287**, 122–129.
26 Y. Lin, K. Sun, S. Liu, X. Chen, Y. Cheng, W. C. Cheong, Z. Chen, L. Zheng, J. Zhang and X. Li, *Adv. Energy Mater.*, 2019, **9**, 1901213.
27 Z. Wang, J. Yang, W. Wang, F. Zhou, H. Zhou, Z. Xue, C. Xiong, Z.-Q. Yu and Y. Wu, *Sci. China Mater.*, 2021, **64**, 861–869.
28 P. He, X. Y. Yu and X. W. Lou, *Angew. Chem., Int. Ed.*, 2017, **56**, 3897–3900.
29 L. Wu, L. Yu, F. Zhang, B. McElhenny, D. Luo, A. Karim, S. Chen and Z. Ren, *Adv. Funct. Mater.*, 2021, **31**, 2006484.
30 Y. Zhao, J. Zhang, Y. Xie, B. Sun, J. Jiang, W.-J. Jiang, S. Xi, H. Y. Yang, K. Yan and S. Wang, *Nano Lett.*, 2021, **21**, 823–832.
31 Y. Jin, S. Huang, X. Yue, H. Du and P. K. Shen, *ACS Catal.*, 2018, **8**, 2359–2363.
32 K. Zhan, C. Feng, X. Feng, D. Zhao, S. Yue, Y. Li, Q. Jiao, H. Li and Y. Zhao, *ACS Sustain. Chem. Eng.*, 2020, **8**, 6273–6281.